B-spline function-based approach for GPS tropospheric tomography

Haji-Aghajany, Saeid; Amerian, Yazdan; Verhagen, Sandra

DOI
10.1007/s10291-020-01005-x

Publication date
2020

Document Version
Accepted author manuscript

Published in
GPS Solutions

Citation (APA)
Haji-Aghajany, S., Amerian, Y., & Verhagen, S. (2020). B-spline function-based approach for GPS tropospheric tomography. *GPS Solutions*, *24*(3), Article 88. https://doi.org/10.1007/s10291-020-01005-x

B-spline function-based approach for GPS tropospheric tomography

Saeid Haji-Aghajany[a,b], Yazdan Amerian[a], Sandra Verhagen[b]

[a]Faculty of Geodesy and Geomatics Engineering, K. N. Toosi University of Technology, Tehran, Iran

[b]Faculty of Civil Engineering and Geosciences, Delft University of Technology, Stevinweg 1, 2628 CN Delft, The Netherlands

s_h_aghajany@mail.kntu.ac.ir, S.HajiAghajany@tudelft.nl, amerian@kntu.ac.ir, sandra.verhagen@tudelft.nl

Abstract Tropospheric tomography is one of the most important techniques to reconstruct three dimensional (3D) images of the tropospheric water vapor fields using a local GNSS network. In the conventional tropospheric tomography method, called voxel-based tropospheric tomography, the 3D space is divided into many voxels and the amount of water vapor is estimated for each voxel. This method suffers from three disadvantages. First, it needs empirical constraints in order to fix the rank deficiency of the coefficient matrix. Second, the amount of water vapor is assumed to be constant in the 3D space of a voxel despite the large spatial variations of this parameter. Third, the number of unknown parameters is high compared to the number of observations. Therefore, an approach based on mathematical functions, called function-based tropospheric tomography, is presented to overcome these problems. The tropospheric tomography using the voxel-based and function-based approaches is performed using 17 GPS stations and different weather conditions have been considered. Radiosonde observations and GPS positioning results are used to validate the obtained results. Comparison of the results with the radiosonde data indicates that the use function-based method reduces the mean RMSE by about 0.3 gr/m^3. Validation using positioning shows that in wet weather conditions, the difference between the RMSE of the two approaches is significant. All the validations show the ability and applicability of the function-based tropospheric tomography approach.

Keywords: GPS, Tropospheric tomography, Water vapor, Function-based, B-spline

Introduction

The spatiotemporal distribution of water vapor is very important in numerical weather forecasting and disastrous-weather monitoring. There are many instruments for measuring water vapor, such as radiosonde, water vapor radiometer, and meteorological satellites and sensors (Merrikhpour and Rahimzadegan 2017; Merrikhpour and Rahimzadegan 2019). These instruments have low spatiotemporal resolution and high cost and are dependent on weather conditions. In recent years, the GNSS tropospheric tomography has been used to retrieve the 3D distribution of water vapor and to overcome the mentioned drawback of the instruments. The first GNSS tropospheric tomography experiments to obtain wet refractivity were performed by Flores and Hirahara (Flores et al. 2000; Hirahara 2000). In the following years, many researchers have tried to improve the accuracy and performance of this technique (Bender et al. 2011; Perler et al. 2011; Rohm et al. 2014; Yao and Zhao 2016; Haji-Aghajany and Amerian 2017; Haji-Aghajany and Amerian 2018; Zhao et al. 2018a; Heublein et al. 2019).

In voxel-based tropospheric tomography, due to the geometric distribution of GNSS receiver and the constellation of GNSS satellites, some voxels are not crossed by any ray. This problem causes a rank deficiency in the coefficient matrix. Some previous researchers proposed the methods of using the signals penetrating from the side face of tomography area (Yao and Zhao 2016; Zhao and Yao 2017; Zhao et al., 2020) and using the data of GNSS observations outside the study area to solve this problem (Zhao et al., 2019). However, in general, the use of constraints to solve the problem is inevitable. Some researchers have suggested approaches to add constraints to the tropospheric tomography problem (Flores et al. 2000; Troller et al. 2002; Rohm and Bosy 2009; Bender et al. 2011). These empirical constraints sometimes cause the reconstructed water vapor field to deviate from the correct distribution. Considering the amount of water vapor fixed everywhere in the 3D space of a voxel and the high number of unknown parameters compared to the number of observations are other drawbacks of the conventional tropospheric tomography method. The high number of unknown parameters reduces the stability of the tomography model.

The first function-based tropospheric tomography studies of water vapor have been performed by Zhao et al. (2018b). He used the fix-degree polynomial function for different vertical layers. A high-degree polynomial as an interpolant function oscillates between data points and at the edges of an interval and reduces the accuracy of modeling. We present a new method based on the non-identical degrees of the B-spline scaling function to overcome the disadvantages of the voxel-based and polynomial function-based methods. The B-spline function has already been used in ionosphere tomography and has shown high ability in ionosphere modeling (Amerian et al. 2013a, b). Here, the B-spline scaling function with different degrees and resolution levels is used in the tropospheric tomography.

Function-based tropospheric tomography avoids the use of empirical constraints, and only an a priori constraint is needed to reconstruct the vertical distribution of water vapor. Moreover, it reduces the number of unknown parameters. To perform the tomography, we used the observations of 17 GPS stations for 30 different days under different weather conditions. After applying the voxel-based and function-based methods, the results are validated using the GNSS positioning technique and radiosonde observations. In the following, the basics of the voxel-based and function-based tropospheric tomography are provided. Then, the study area, data set, and the obtained results from the two tomography approaches are presented. Validation and discussion are presented in the last section.

Tropospheric tomography technique

The slant water vapor (SWV) is the total water vapor content from satellite to receiver. This can be one of the input data types of the tomography problem and is expressed as follows (Braun 2004):

$$SWV = \int_{\mathrm{Rec.}}^{Sat.} \rho(s)\, ds \tag{1}$$

where s represents the path of the ray, and ρ is the water vapor density (WVD). Equation (1) is the fundamental relation of the tropospheric tomography problem. The SWV can be obtained by the following formula (Bevis et al. 1992):

$$SWV = \frac{10}{R_w[(k_3 / T_m) + k_2^{'}]} SWD \tag{2}$$

where $k_2^{'} = 16.48\ \text{KhPa}^{-1}$, $k_3 = 3.776\times10^5\ \text{K}^2\text{hPa}^{-1}$ and $R_w = 461\ \text{JKg}^{-1}\text{K}^{-1}$ are refractivity coefficients. T_m is weighted mean tropospheric temperature and *SWD* is the slant wet delay of the ray which can be computed using (Davis et al. 1993):

$$SWD = (m\,f_{wet} \times ZWD) + (mf_{wet} \times \cot(\alpha) \times ((G_{NS}^{W} \times \cos az) + (G_{EW}^{W} \times \sin az))) + R \tag{3}$$

where G_{NS}^{W} and G_{EW}^{W} are non-hydrostatic delay gradients in N-S and E-W directions, mf_{wet} is non-hydrostatic mapping function, α is satellite elevation and az is the azimuth. *ZWD* is the zenith wet delay, which can be estimated by subtracting the zenith hydrostatic delay (ZHD) from the zenith total delay (ZTD). ZHD can be computed accurately using the following model (Saastamoinen 1973):

$$ZHD = \frac{0.002277\ P_s}{(1\text{-}0.00266\ \cos(2\varphi)\ -\ 0.00000028\,H)} \tag{4}$$

where φ and H are the latitude and height and P_s is the surface pressure. In the following, the theory of voxel-based and function-based tomography are described.

Voxel-based method

The tomography area is divided into several voxels in which the WVD is considered a constant during the specified period of time. Therefore, the equation between the SWV and the WVD can be discretized as follows (Chen and Liu 2014):

$$SWV^{P} = \sum_{i}^{n}\sum_{j}^{m}\sum_{k}^{q}\ d_{i,j,k}^{P}\,\rho_{i,j.k} \tag{5}$$

where *n, m* and *q* is the number of voxels in the latitudinal, longitudinal, and vertical directions, *P* is the counter of rays, $d_{i,j.k}^{P}$ is the distance traveled by the ray *P* in the voxel (i, j, k) and $\rho_{i,j,k}$ is the WVD in the voxel (i, j, k). Equation (5) in matrix form is:

$${}_{T}L_{1} = {}_{T}A_{nmq\ \ nmq}\,\rho_{1} \tag{6}$$

where *T* is the number of the GNSS rays, *A* is the coefficient matrix and ρ is the vector of unknown WVD. An inversion algorithm needs to be applied to solve the unknown parameters. As previously mentioned, in voxel-based tomography, the coefficient matrix is a large sparse matrix, and not all of the unknowns can be estimated. Therefore, adding constraints using various approaches to solve this problem is inevitable (Flores et al. 2000; Troller et al. 2002; Rohm and Bosy 2009; Bender et al. 2011). As a result, the accuracy of the results is influenced since the additional constraint cannot completely satisfy the actual situation. In this study, the horizontal constraints are performed based on the assumption that the WVD in a voxel is a mean value of its horizontally nearest neighbors (Yao and Zhao 2016). In order to form the vertical constraints, the negative exponential function is used (Flores et al. 2000).

The model resolution matrix is used to select the optimal resolution and geometry for the tomography model (Haji-Aghajany and Amerian 2017). The 3D ray-tracing technique is used to compute the distance traveled by the rays in each voxel. More details about this technique can be found in Haji-Aghajany and Amerian (2017). The tropospheric tomography is a large and ill-conditioned inverse problem due to the high number of observations and a wide area of modeling. Therefore the use of regularization methods is necessary. We use the least-squares QR (LSQR) iterative regularization method (Haji-Aghajany and Amerian 2017; Haji-Aghajany and Amerian 2018).

Function-based method

In previous studies, the study area was divided into many voxels, which caused problems in the determination of the WVD. In the function-based tropospheric tomography, the study area is not divided in the horizontal direction, and only a few vertically layers are needed. In this method, the WVD for each layer is expressed as a function:

$$\rho = F(\lambda, \varphi) \tag{7}$$

where λ and φ are the longitude and latitude of intersection between the ray and the center of the layer. Therefore, the SWV for *i*-th layer in *P*-th ray direction can be written as:

$$SWV_i^P = \rho_i . d_i^P = F(\lambda_i, \varphi_i) . d_i^P \tag{8}$$

where ρ_i is the WVD for the location of (λ_i, φ_i) and d_i^P is the distance travel by the *P*-th ray in *i*-th layer. The SWV can be transformed as follows:

$$SWV^P = SWV_1^P + SWV_2^P + \ldots + SWV_n^P \tag{9}$$

Using to equation (8), this can be written as follows:

$$SWV^P = F(\lambda_1,\varphi_1).d_1^P + F(\lambda_2,\varphi_2).d_2^P + \ldots + F(\lambda_n,\varphi_n).d_n^P \tag{10}$$

where n is the number of layers. It is clear that the distribution of WVD at the different elevation layers is not the same. Therefore, it is better to use various degree functions for different layers. Accordingly, equation (10) can be written as follows:

$$SWV^P = F_1(\lambda_1,\varphi_1).d_1^P + F_2(\lambda_2,\varphi_2).d_2^P + \ldots + F_n(\lambda_n,\varphi_n).d_n^P \tag{11}$$

Basic schematic diagram of this method can be seen in Fig.1.

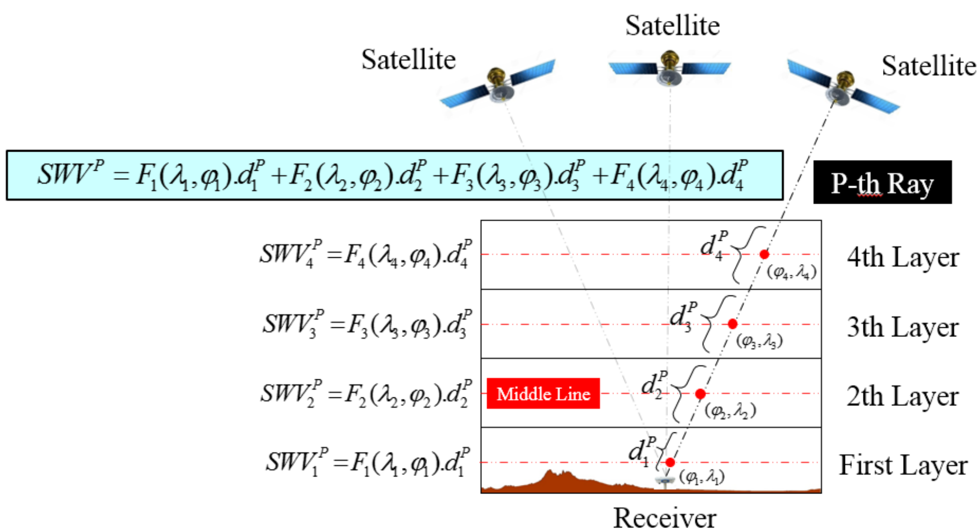

Fig. 1 Schematic diagram of four-layer function-based tropospheric tomography

B-spline function

Due to the spatial variations of water vapor and considering the local modeling ability of different functions, the B-spline function is used as the base function for regional modeling of the WVD. B-spline is a special kind of wavelet that presents useful and remarkable properties such as symmetry, simplicity, semi-orthogonality, and compact support (Amerian et al. 2013a). The normalized B-spline scaling function is as follows:

$$\phi_{J,k}(x) = N_{J,k}^{d}(x) = \frac{x - t_k^J}{t_{k+d}^J - t_k^J} N_{J,k}^{d-1}(x) + \frac{t_{k+d+1}^J - x}{t_{k+d+1}^J - t_{k+1}^J} N_{J,k+1}^{d-1}(x) \tag{12}$$

where d is degree of function, J is resolution level, k is shift and x is variable. The scaling function space has $K_J = 2^J + d$ basis functions. It should be noted that when the denominators of (12) are zero, the fraction will be considered zero (Amerian et al. 2013a). The required initial values can be obtained using:

$$N_{J,k}^{0}(x) = \begin{cases} 1 & if \quad t_k^J \le x \le t_{k+1}^J \\ 0 & otherwise \end{cases} \tag{13}$$

where $k = 0, 1, ..., K_J - 1$ are shift values and $t_0, t_1, ..., t_{K_J+d}$ is a sequence of spaced values called knots.

$$t_0, t_1, ..., t_{K_J+d} = \frac{1}{2^J}\left(\underbrace{0, ..., 0}_{d+1\ times}, 1, 2, ..., 2^J - 1, \underbrace{2^J, ..., 2^J}_{d+1\ times} \right) \tag{14}$$

In this method, endpoint-interpolating B-spline on unit interval [0,1] is used to avoid the edge effect at the boundaries. For this aim, the first and last d+1 knots are set to zero and one, respectively (Mautz et al. 2005; Amerian et al. 2013a; Amerian et al. 2013b).

The WVD in each layer is expanded into 2D B-spline scaling function $\phi_{J_1 J_2 k_1 k_2}(\lambda, \varphi)$ with unknown scaling coefficients $C_{J_1 J_2 k_1 k_2}$:

$$\rho_i = \sum_{k_1=0}^{K_{J_1-1}} \sum_{k_2=0}^{K_{J_2-1}} C_{J_1 J_2 k_1 k_2} \phi_{J_1 J_2 k_1 k_2}(\lambda_i, \varphi_i) \tag{15}$$

The 2D B-spline scaling function can be computed using the tensor product of 1D functions:

$$\phi_{J_1 J_2 k_1 k_2}(\lambda, \varphi) = \phi_{J_1, k_1}(\lambda)\, \phi_{J_2, k_2}(\varphi) \tag{16}$$

Finally, the tropospheric tomography based on 2D B-spline scaling function is expressed as follows:

$$SWV^P = (d_1^P . \sum_{k_1=0}^{K_{J_1-1}} \sum_{k_2=0}^{K_{J_2-1}} C^1_{J_1 J_2 k_1 k_2}\ \phi_{J_1 J_2 k_1 k_2}(\lambda_1, \varphi_1)) + ... + (d_n^P . \sum_{k_1=0}^{K_{J_1-1}} \sum_{k_2=0}^{K_{J_2-1}} C^n_{J_1 J_2 k_1 k_2}\ \phi_{J_1 J_2 k_1 k_2}(\lambda_n, \varphi_n)) \tag{17}$$

This system of equations can be written in the following form:

$$L = A\,x \tag{18}$$

where L is the observation vector, A is the coefficient matrix that includes the base functions and distance traveled by the rays in each layer, and x is an unknown vector that includes the B-spline scaling coefficients. The B-spline scaling function provides local support, and not all observations will contribute to the estimation of an unknown. Therefore, the coefficient matrix A is a sparse matrix. In this method, it is necessary to use a prior constraint in order to reconstruct the vertical distribution of water vapor properly. For this purpose, the radiosonde measurements at various layers have been used. The tropospheric tomography is inherently a Fredholm integral equation of the first kind. In mathematics, it has been shown that in this kind of integral equation, the output is not a continuous function of the input parameters (Hansen 1997). It can be proven that inverse problems based on this kind of integral equation are ill-conditioned problems, and the use of regularization methods to solve them is inevitable (Hansen 1997). Similar to the voxel-based approach, the LSQR iterative regularization method is used to solve the inverse problem. The 3D ray-tracing technique is used to compute the distance traveled by the rays in each layer.

Study area and data set

In order to study the function-based tropospheric tomography method, a region in North America has been selected (Fig.2). For a comprehensive review of the effectiveness of the proposed method, 17 dual-frequency GPS observations for 30 days of 2018 between July and December in different weather conditions have been used. These days have been selected based on the diversity of the relative humidity index. The distribution of the GPS stations and topography of the study area can be seen in Figs.3 and 4. In this research, the ERA-Interim reanalysis model published by the European Center for Medium-Range Weather Forecasts (ECMWF) has been used to perform 3D ray-tracing technique and to select appropriate degree and level in function-based tomography. The ERA-Interim reanalysis model presented values of several meteorological data on 37 pressure levels. The spatial resolution of this data is about 75 km (Dee et al. 2011). These data have been widely used in various aspects of geodesy and remote sensing (Haji-Aghajany et al., 2017; Haji-Aghajany et al., 2019). The results are validated using observations from the radiosonde station in the area in addition to the positioning technique.

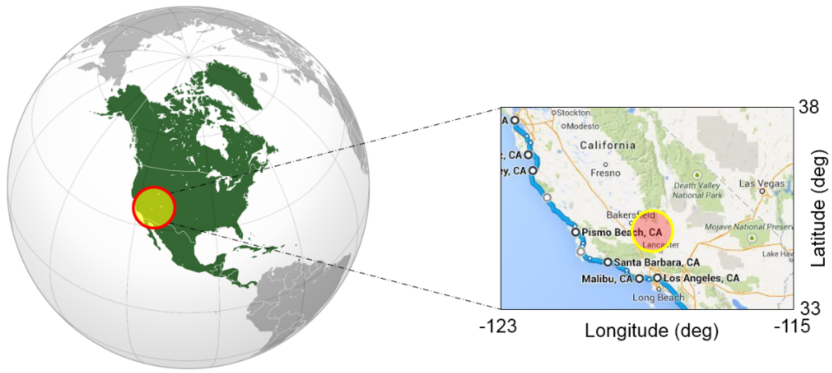

Fig. 2 Geographical location of the study area

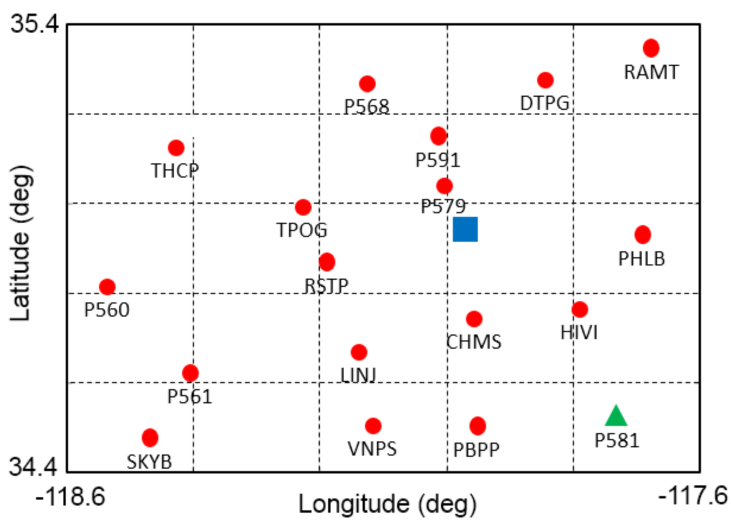

Fig. 3 Distribution of the GPS stations. The blue square represents the radiosonde station, and the green triangle shows the position of the station used to evaluate the results

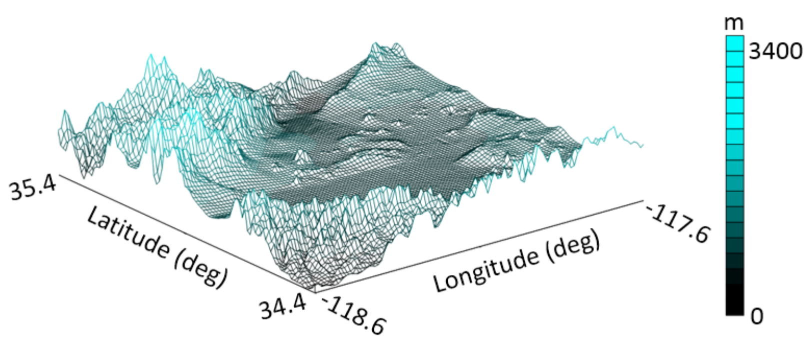

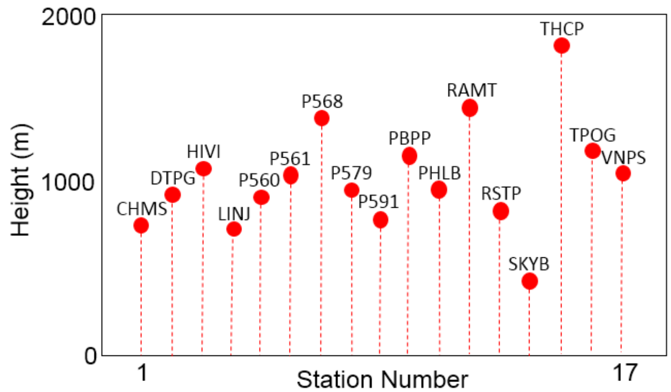

Fig. 4 Topography of the study area and vertical distribution of the GPS stations.

Data processing and results

The GPS observations have been processed using Bernese 5.2 software to estimate the tropospheric delay (Dach et al. 2015). First, the RNXSMT program has been used to detect cycle slip and outlier. The next step was to convert the RINEX (Receiver Independent Exchange) ASCII format observation files format to the software format using RXOBV3 program. Then, the standard orbits have been created using PRETAB and ORBGEN programs. CODSPP and MAUPRP programs have been used for clock synchronization and to resolve cycle slip and multipath, respectively. Finally, GPSEST program has been used to parameter determination (Dach et al. 2015). The ionosphere-free linear combination, a ZTD interval of 30 minutes and gradients interval in north-south and east-west directions of 2 hours have been considered for this processing. The global mapping function (GMF) has been used to convert the zenith direction to slant direction (Bohm and Niell, 2006). Examples of obtained ZTDs can be seen in Fig.5. The different behavior of the delay in these stations are due to the topography of the area and different weather conditions.

The RESRMS program can be used to screen the post–fit residuals produced in a GPSEST run to identify outliers. In the following, the results of voxel-based and function-based tomography are presented.

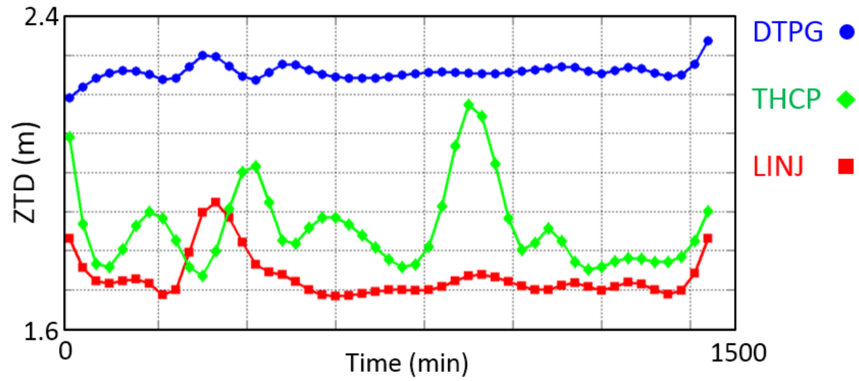

Fig. 5 Computed ZTD for the three sample stations on one of the processing days

Voxel-based tomography results

One of the most important steps of voxel-based tropospheric tomography is selecting the optimum horizontal and vertical resolution for the model according to the topography of the study area. The model resolution matrix is one of the characteristics of the coefficient matrix and reflects the geometry and optimal resolution of the tomography model (Bender et al. 2011; Haji-Aghajany and Amerian. 2017). According to the resolution matrix, the horizontal resolution of 0.2 degrees has been chosen for the tomography model (Fig.6). The vertical resolution for the first 6 layers is 500 meters. This resolution is reduced to 1000 meters for the next 4 layers in the figure.

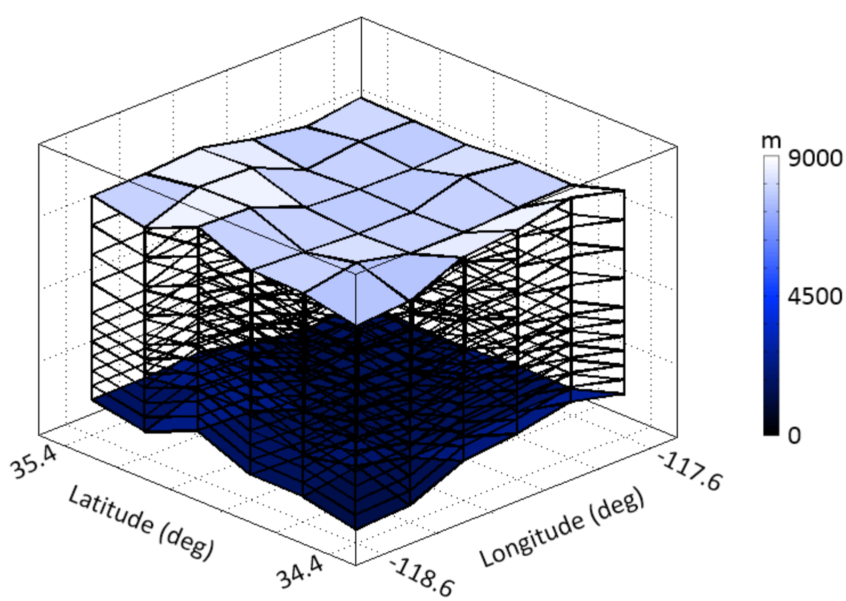

Fig. 6 3D voxel-based tomography model

Based on all the above, the 3D WVD fields have been reconstructed for 30 days under different weather conditions. The voxel-based tropospheric tomography results of this research have a temporal resolution of 30 min following the temporal resolution of the estimated tropospheric delay. An example of the obtained WVD field in different layers can be seen in Fig.7. The WVD has an irregular spatiotemporal distribution due to the advection, turbulence and transport. The distribution of the WVD in vertical layers for three epochs is well visible in the figure. It is correctly seen that the WVD decreases with increasing height. The important point in the figure is that the WVD is the same everywhere in the 3D space of a voxel.

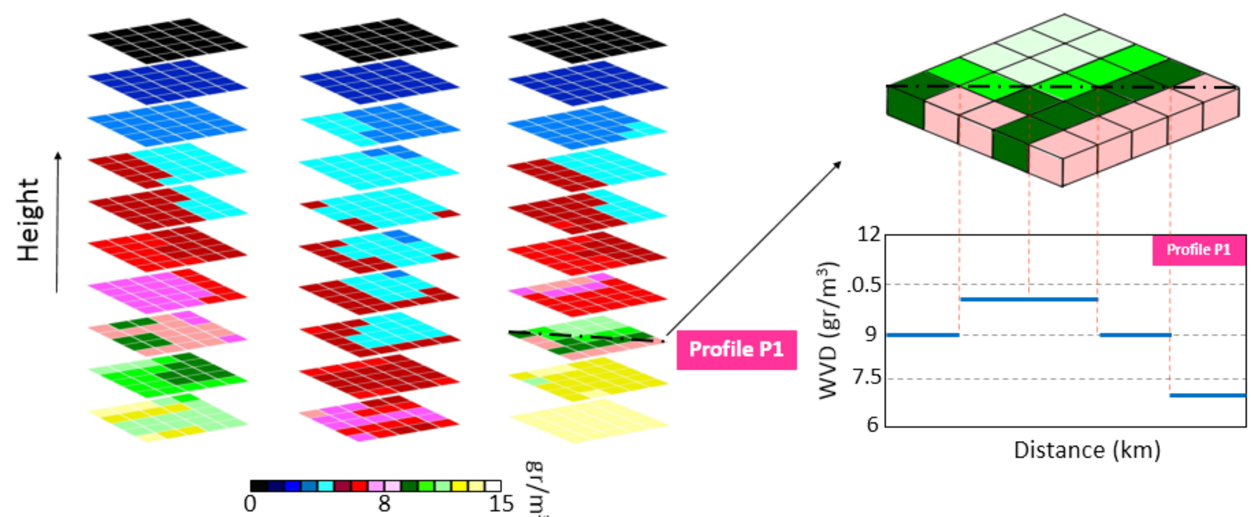

Fig. 7 Example of reconstructed WVD field for three different epochs (07/08/2018-03/10/2018-02/11/2018). The plotted profile shows that the reconstructed water vapor obtained from this method is constant in each voxel

Function-based tomography results

In order to perform function-based tropospheric tomography, we have considered the vertical resolution of the model following the previous method. The most important step in the function-based tropospheric tomography is to select the optimal degree and level of the B-spline function.

The spatial distribution of WVD varies at different height levels. At higher vertical layers, the spatial variations of WVD are smoother compared to the lower layers. Therefore it is necessary to use different degrees and levels of B-spline function in each layer for better modeling of WVD as well as better management of the number of unknown parameters. The ERA-Interim model has been used to determine the appropriate degree and level in different vertical layers. For this purpose, the B-spline functions with different degrees and levels have been fitted to one year of ERA-Interim data, and then the coefficients of the functions have been computed. The ERA-Interim data of 10 days in different weather conditions and different average relative humidity have been used to evaluate different degrees and levels of the function in various vertical layers. Fig.8 shows the comparison of the average Root Mean Square Error (RMSE) between the obtained WVD using the function coefficients and the ERA-Interim data which indicates the model misfit.

Based on these results and considering the number of unknown parameters produced by the B-spline function, the optimal degrees and levels of the function in different vertical layers have been chosen to perform the method. Figure 9 shows the intended degree and level and the number of unknown parameters in each layer.

Figure 10 shows the example of the estimated WVD field in vertical layers for three different epochs using the B-spline function-based method in the study area. The 2D distribution of WVD and profile plotted in the figure shows that the function-based tomography models results are more detailed and continuous compared to the general and discrete results of the voxel-based method. In order to compare the two methods and to obtain more precise conclusions, the obtained results should be validated.

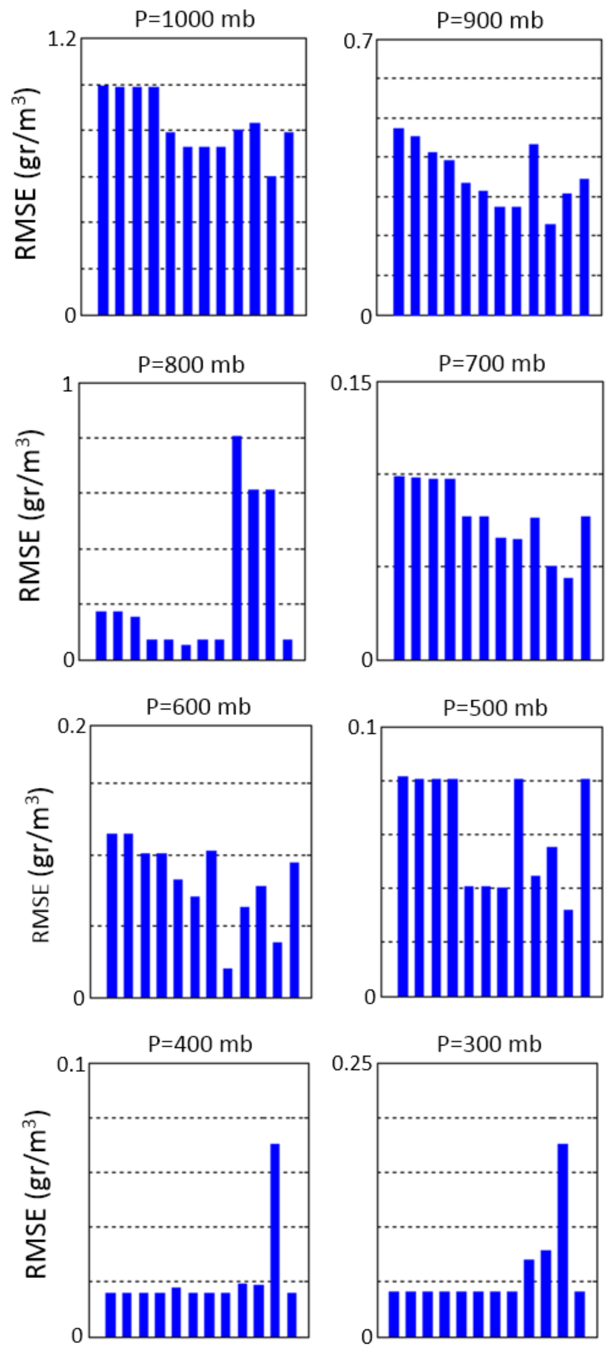

P=1000 mb
1.2
0
RMSE (gr/m3)
P=900 mb
0.7
0
P=800 mb
1
0
RMSE (gr/m3)
P=700 mb
0.15
0
P=600 mb
0.2
0
RMSE (gr/m3)
P=500 mb
0.1
0
P=400 mb
0.1
0
RMSE (gr/m3)
P=300 mb
0.25
0

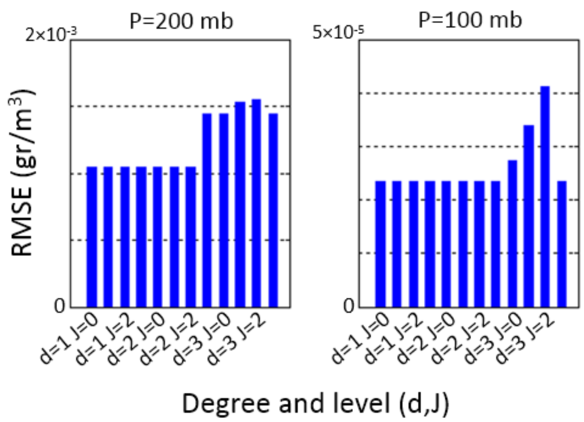

Fig. 8 Comparison between obtained average RMSE from different degrees and levels at some pressure levels. This comparison shows that the average RMSE decreases with decreasing pressure.

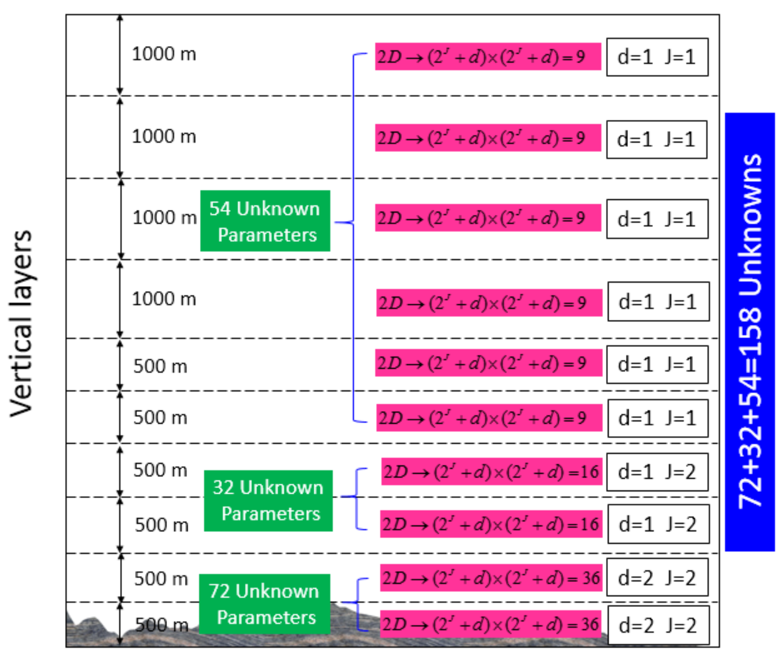

Fig. 9 Schematic diagram of the considered layer and the number of unknown parameters

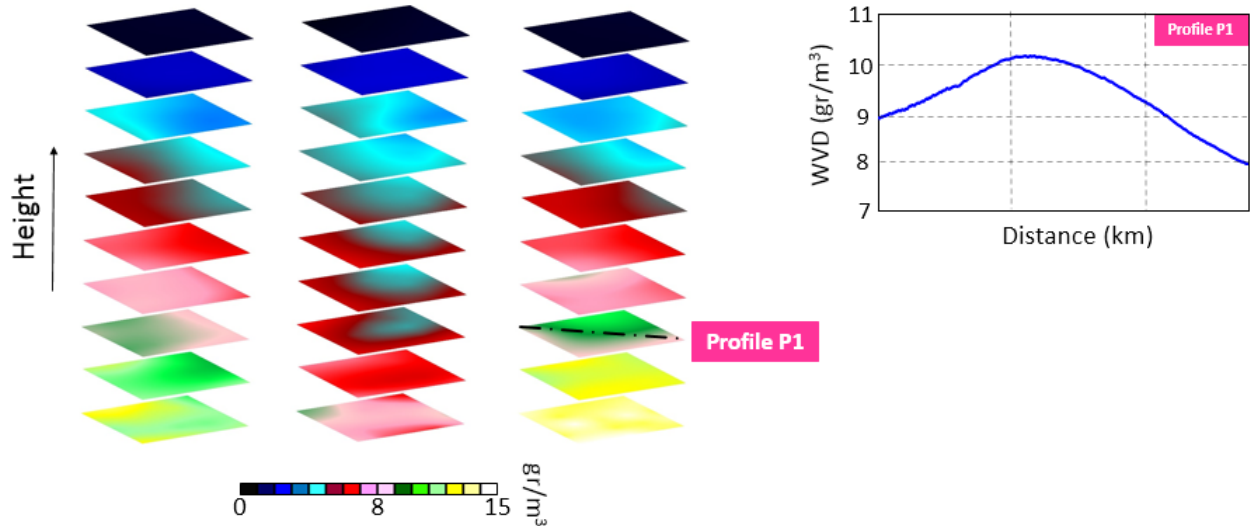

Fig. 10 Example of obtained WVD field for three different epochs (07/08/2018-03/10/2018-02/11/2018).

Validation of the tomography modeling

Radiosonde observations can provide accurate WVD profiles. Therefore, the use of these data is one of the most common ways to validate the results of tropospheric tomography. Radiosonde balloons are usually launched daily at 00:00 and 12:00 UTC. There is a radiosonde station located in the study area. In order to validate the WVD from voxel-based and functioned-based methods, we compared the results for the location of the radiosonde station with radiosonde data (as reference) for the experimental period of 30 days. Examples of this comparison for six different epochs are visible in Fig.11. The reconstructed WVD is generally consistent with radiosonde measurements. However, at some altitudes, significant differences between the obtained WVD and validation data are visible. The maximum differences between the reconstructed WVD and the radiosonde measurements are visible in the lower and middle vertical layers. Table.1 shows the statistical parameters between the results of tropospheric tomography methods and radiosonde data over the tested period. The scatter plot has been used to better compare the obtained WVD (Fig.12).

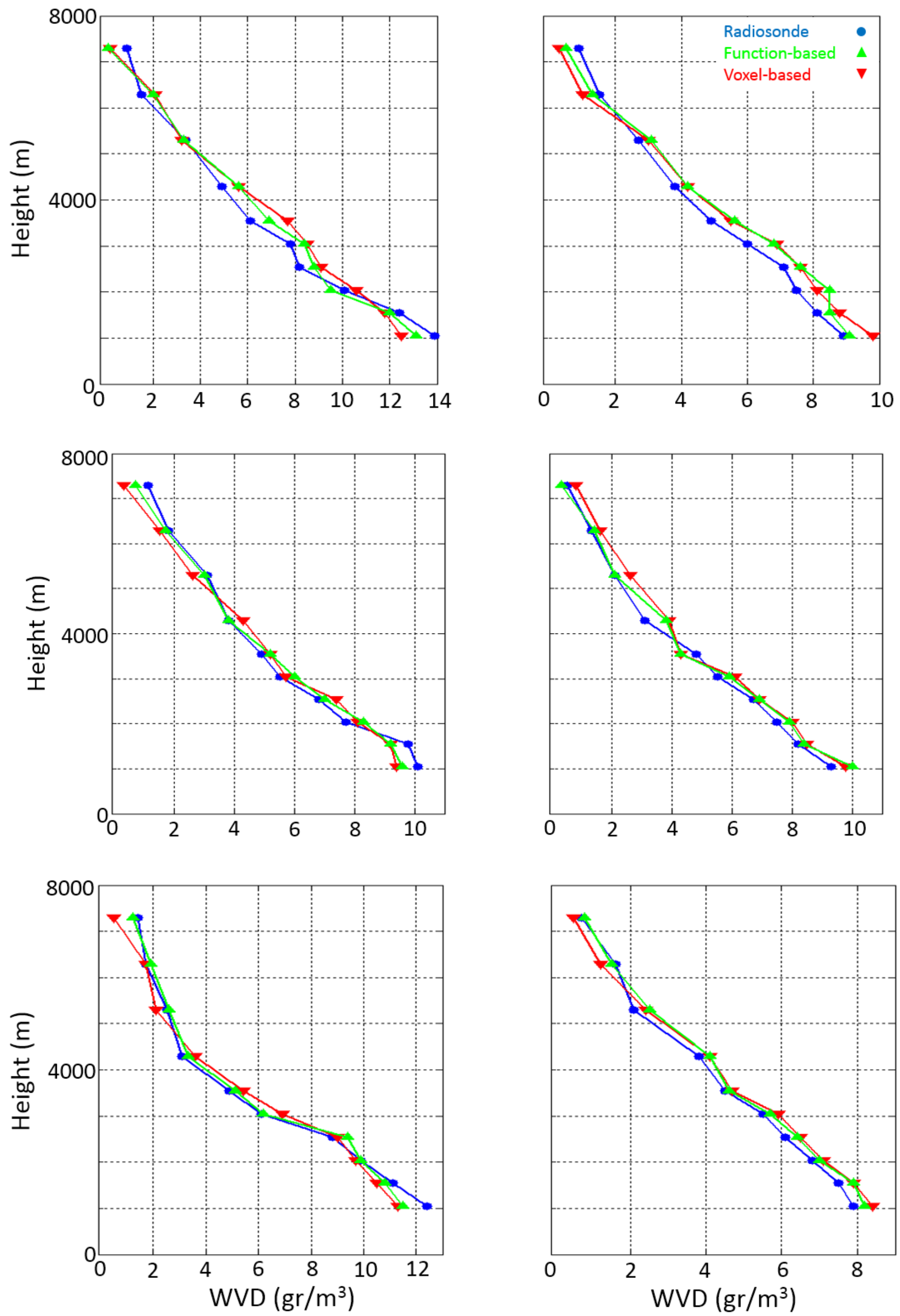

Fig. 11 Examples of comparison between reconstructed WVD and radiosonde measurements for three different epochs (07/08/2018-03/10/2018-02/11/2018).

Table1 Statistical comparison between the reconstructed WVD and radiosonde validation data

Method	RMSE (gr/m^3)	Bias (gr/m^3)	Min-Diff (gr/m^3)	Max-Diff (gr/m^3)
Function-based	0.61	-0.14	0.06	0.91
Voxel-based	0.89	-0.15	0.11	1.62

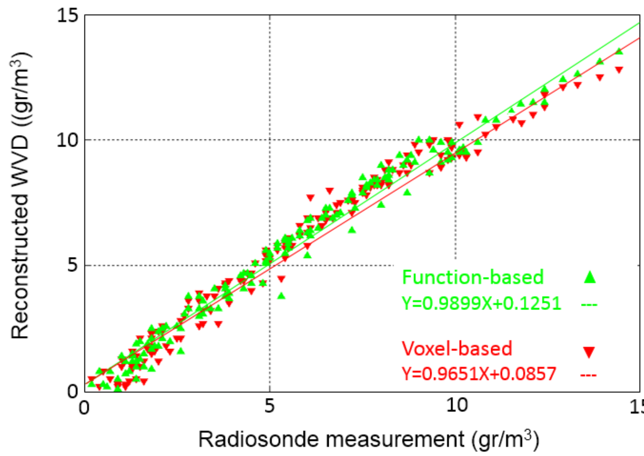

Fig. 12 Scatter plot between reconstructed WVD and radiosonde observations

The statistical results in Table.1 and the slope of the fitted lines in Fig.12 show that the results obtained from the two approaches are close to each other, although the results of the function-based method are closer to the radiosonde observations. The used radiosonde station is located in the middle of the study area, so the obtained results on the boundary voxels of the tomography model cannot be validated using this station. On the other hand, in order to compare these two methods more precisely, it is necessary to examine the results on the sides of the tomography model. Therefore, the precise point positioning (PPP) technique has been used for this purpose.

One GPS station in the selected area has been used for this validation. It should be noted that this station has not been used in the tomography process. First, the position time series of this station on the days of tomography has been obtained from the Plate Boundary Observatory (PBO) GPS network (http://unavco.org). Fig.13 shows the time series of the position components of this station. The SWD and slant hydrostatic delay (SHD) of GPS observations has been estimated using reconstructed water vapor from two tomography methods and saastamoinen model, respectively. Then, the observations of the GPS station have been corrected using these corrections. After this step, positioning has been performed again using the PPP technique. Previous studies have proven that the discrepancy between tropospheric effect correction methods is more noticeable in wet weather conditions. Therefore, the comparison has been made in two types of weather conditions. The first category includes days with an average humidity of more than 50%, and the second group includes days with an average humidity of less than 50%. This classification has been done based on the ERA-Interim data. Fig.14 shows the comparison between obtained 3D positions from two tomography methods. Finally, the RMSE between the positions obtained using the two tomography methods and the position obtained from the PBO GPS network has been computed (Fig.15, Table.2).

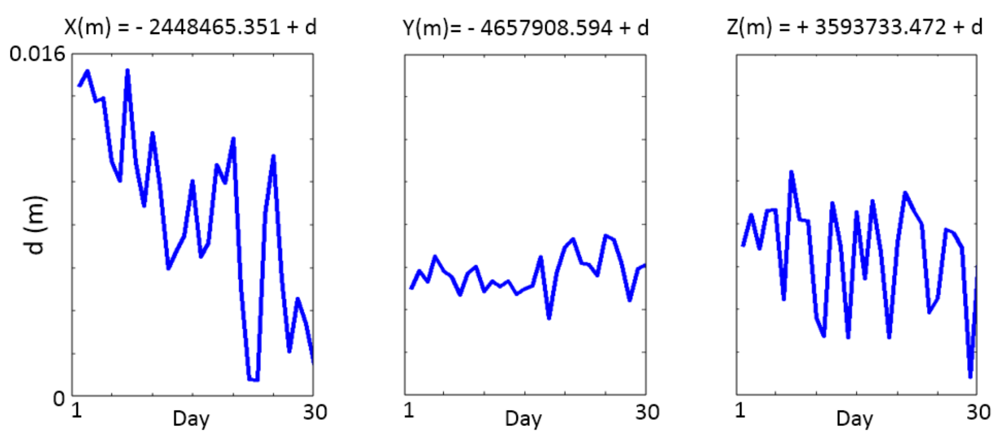

Fig. 13 Position time series of this station

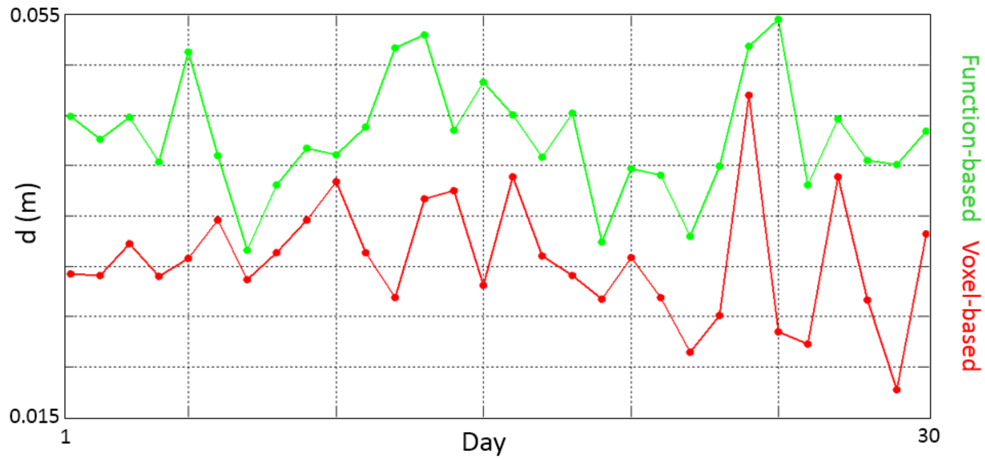

Fig. 14 3D difference between obtained positions from two tomography methods and the positions obtained from the PBO GPS network

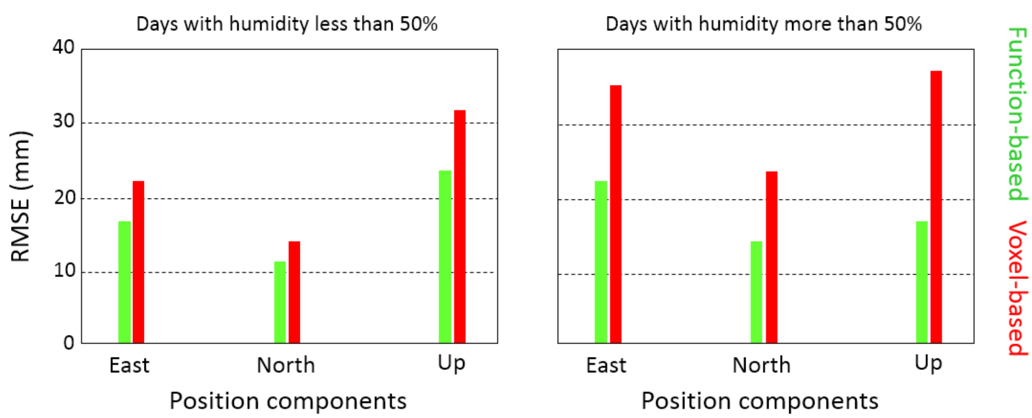

Fig. 15 RMSE in different weather condition

Table2 Comparison of the obtained RMSE

	RMSE in Days with humidity less than 50% (mm)			**RMSE in Days with humidity more than 50% (mm)**		
	East	North	Up	East	North	Up
Function-based	16.92	11.83	23.58	22.12	14.47	17.51
Voxel-based	22.71	14.87	31.97	35.86	23.53	37.71

On days with humidity less than 50%, the difference between obtained RMSE in computing the Up component is about 9 mm. This difference is statistically significant. However, the obtained RMSE of the East and North components for both tomography methods is very close to each other, and there is some improvement in the accuracy of the results. This comparison shows that accuracy improvement in the vertical component is more significant than in the horizontal components.

On days with humidity more than 50%, the conclusion is quite different. The difference between the RMSE in East, North and Up components is about 14, 10 and 20 mm, respectively. Considering the accuracy of the PPP technique, these differences are significant and cannot be ignored. The highest and lowest differences are observed in the Up and East components. On the basis of Fig.14, it can be generally said that the effect of using the method to increase the accuracy of the Up and East components are significant.

Based on all these validations, it can be concluded that using the function-based method based on B-spline function can increase the ability of the tomography technique compared to the voxel-based method.

Conclusion

We presented a new tropospheric tomography approach based on the B-spline function and its ability was validated under different weather conditions. This function-based method divided the research area for some layers vertically while the WVD function was introduced horizontally, rather than discretized the research area into many voxels as performed by the voxel-based method. Using the function-based tropospheric tomography, we can neglect the empirical constraints. This method only uses an a priori constraint. The empirical constraints have an unfavorable effect on voxel-based tomography results due to the unsuitable relationship between voxels in vertical and horizontal directions. The proposed method also reduces the number of unknown parameters because it estimates only the coefficients of the WVD function in each vertical layer. Therefore, this method can overcome the rank deficiency problem in tropospheric tomography resolution. It was observed that using the function-based method, the WVD can be reconstructed continuously in each vertical layer, unlike the voxel-based method. The results of two tomography methods were compared using radiosonde observations and the PPP technique. Validation using radiosonde showed that the function-based method is more accurate in reconstructing the water vapor. However, the results of the two methods were close to each other. Next, the PPP technique was used to evaluate the results near the edge of the tomography model. The results of this validation showed that the PPP with a priori data from function-based tomography has better accuracy of the position components (especially Up) than if we take them from voxel-based tomography.

Acknowledgments

The authors would like to appreciate the UNAVCO for the GPS observations and for providing high-accuracy station position time series. We are also grateful to the ECMWF for publishing ERA-Interim data.

Data Availability

The datasets generated during and/or analyzed during the current study are not publicly available but are available from the corresponding author on reasonable request.

References

Amerian Y, Hossainali MM, Voosoghi B., (2013a). Regional improvement of IRI extracted ionospheric electron density by compactly supported base functions using GPS observations. J Atmos Sol Terr Phys 92:23–30. doi: 10.1016/j.jastp.2012.09.011.

Amerian, Y., Voosoghi, B., Mashhadi Hossainali, M., (2013b). Regional Ionosphere Modeling in Support of IRI and Wavelet Using GPS Observations. Acta Geophysica. 61(5):1246-1261, DOI: 10.2478/s11600-013-0121-5.

Bender, M., Dick, G., Ge, M., Deng, Z., Wickert, J., Kahle, H.-G., Raabe, A., and Tetzlaff, G., (2011). Development of a GNSS water vapour tomography system using algebraic reconstruction techniques, Adv. Space Res., 47, 1704–1720.

Bevis, M., Businger, S., Herring, T. A., Rocken, C., Anthes, R. A., Ware, R. H., (1992). GPS meteorology: Remote sensing of atmospheric water vapor using the Global Positioning System. Journal of Geophysical Research: Atmospheres, 97(D14): 15787-15801.

Böhm, J.; Niell, A.; Tregoning, P.; Schuh, H. Global Mapping Function (GMF): A new empirical mapping function based on numerical weather model data. Geophys. Res. Lett. 2006, 33, 1-4.

Braun, J.J., (2004). Remote sensing of atmospheric water vapor with the global positioning system (Ph.D.). University of Colorado.

Chen BY, Liu ZZ., (2014). Voxel-optimized regional water vapor tomography and comparison with radiosonde and numerical weather model. J Geod 88(7):391–703. doi:10.1007/s00190-014- 0715-y.

Dach, R., S. Lutz, P. Walser, P. Fridez (Eds)., (2015). Bernese GNSS Software Version 5.2. User manual, Astronomical Institute, University of Bern, Bern Open Publishing. DOI: 10.7892/boris.72297; ISBN: 978-3-906813-05-9.

J. L. Davis, G. Elgered, A. E. Niell, and C. E. Kuehn., (1993). Ground-based measurement of gradients in the wet radio refractivity of air. Radio Sci., vol. 28, pp. 1003–1038.

Dee, D.P., et al., (2011) The ERA-Interim reanalysis: configuration and performance of the data assimilation system, Q. J. R. Meteorol. Soc. 137(656): 553–597, doi: 10.1002/qj.828.

Flores, A., Ruffini, G., and Rius, A., (2000). 4D tropospheric tomography using GPS slant wet delays, Ann. Geophys. Ger., 18(2):223–234.

Haji-Aghajany. S, B. Voosoghi, and A. Yazdian., (2017). Estimation of North Tabriz Fault Parameters Using Neural Networks and 3D Tropospherically Corrected Surface Displacement Field. Geomatics, Natural Hazards and Risk 8 (2): 918–932. doi:10.1080/19475705.2017.1289248.

Haji-Aghajany, S., Amerian, Y., (2017). Three dimensional ray tracing technique for tropospheric water vapor tomography using GPS measurements. Journal of Atmospheric and Solar-Terrestrial Physics. 164, 81-88. doi: 10.1016/j.jastp.2017.08.003.

Haji-Aghajany, S., Amerian, Y., (2018). Hybrid Regularized GPS Tropospheric Sensing Using 3-D Ray Tracing Technique. IEEE Geoscience and Remote Sensing Letters. 15(10):1475-1479. doi: 10.1109/LGRS.2018.2853183.

Haji-Aghajany. S, B. Voosoghi, and Y. Amerian., (2019). "Estimating the slip rate on the north Tabriz fault (Iran) from InSAR measurements with tropospheric correction using 3D ray tracing technique." Advance in space research. Volume 64, Issue 11, Pages 2199-2208. Doi: https://doi.org/10.1016/j.asr.2019.08.021.

Hansen, P.C., (1997). Rank-deficient and Discrete Ill-posed Problems. Numerical Aspects of Linear Inversion, Monographs on Mathematical Modeling and computation, Vol. 4, SIAM, Philadelphia

Heublein, M., Alshawaf, F., Erdn, Ba., Zhu, X., Hinz, S., (2019). Compressive sensing reconstruction of 3D wet refractivity based on GNSS and InSAR observations, Journal of Geodesy, 93(2):197-217. https://doi.org/10.1007/s00190-018-1152-0.

Hirahara K., (2000). Local GPS tropospheric tomography, Earth Planet. Space, 52:935–939.

Mautz,R., Ping,J., Heki,K., Schaffrin,B., Shum,C.K., Potts,L.,2005. Efficient spatial and temporal representations of global ionosphere maps over Japan using B-spline wavelets. Journal of Geodesy 78,660–667.

Perler D, Geiger A, (2011). Hurter F. 4D GPS water vapor tomography: new parameterized approaches. J Geodesy, 85:539-550.

Merrikhpour, M., Rahimzadegan, M., (2017). Improving the Algorithm of Extracting Regional Total Precipitable Water Vapor Over Land From MODIS Images. IEEE Transactions on Geoscience and Remote Sensing, 55(10):5889-5898. doi: 10.1109/TGRS.2017.2716414.

Merrikhpour, M., Rahimzadegan, M., 2019. Analysis of temporal and spatial variations of total precipitable water vapor in western Iran using radiosonde and MODIS measurements, Journal of Applied Remote Sensing 13(4). https://doi.org/10.1117/1.JRS.13.044508.

Rohm, W. and Bosy, J., (2009). Local tomography troposphere model over mountains area, Atmos. Res., 93:777–783.

Rohm W, Zhang K, Bosy J., (2014). Limited constraint, robust Kalman filtering for GNSS troposphere tomography. Atmos Meas Tech, 6:1475-1486.

Saastamoinen, J., (1973). Contributions to the theory of atmospheric refraction. Part II: refraction corrections in satellite geodesy. Bull. Geod. 107:13–34.

Troller, M., Burki, B., Cocard, M., Geiger, A., Kahle, H. G., (2002). 3-D refractivity field from GPS double difference tomography, Geophys. Res. Lett., 29, 2-1–2-4.

Yao Y, Zhao Q., (2016). Maximally Using GPS Observation for Water Vapor Tomography. IEEE T Geosci Remote, 54, 7185-7196.

Zhao, Q., & Yao, Y. (2017). An improved troposphere tomographic approach considering the signals coming from the side face of the tomographic area. Annales Geophysicae, 35(1), 87-95.

Zhao, Q. Z., Yao, Y. B., Cao, X. Y., Zhou, F., and Xia, P., (2018a). An optimal tropospheric tomography method based on the multi-GNSS observations, Remote Sensing, 10, 1–15.

Zhao, Q.; Yao, Y.; Yao, W., (2018b). Troposphere Water Vapour Tomography: A Horizontal Parameterised Approach. Remote Sens. 10:1241.

Zhao, Q., Zhang K., Yao, Y., and Li, X., and Yao, W. (2019). A new troposphere tomography algorithm with a truncation factor model (TFM) for GNSS networks, GPS Solutions, 2019,23:64,DOI:10.1007/s10291-019-0855-x.

Zhao, Q., Yao, W., Yao, Y., Li, X. (2020). An improved GNSS tropospheric tomography method with the GPT2w model. GPS Solut 24, 60. https://doi.org/10.1007/s10291-020-0974-4.

Author Biographies

Saeid Haji-Aghajany is currently a Ph.D. candidate under the supervision of Dr. Yazdan Amerian at K. N. Toosi University of Technology, Tehran, Iran. He is also a researcher under the supervision of Dr. Sandra Verhagen at the Delft University of Technology. His main research interests include GNSS meteorology, GNSS remote sensing and deformation monitoring using GPS and InSAR observations.

Yazdan Amerian received his B.Sc. degree in geomatics engineering from the University of Tehran and his M.Sc. and Ph.D. degrees in geodesy from K. N. Toosi University of Technology, Tehran, Iran. He is now an assistant professor with the Faculty of Geodesy and Geomatics Engineering, K. N. Toosi University of Technology. His main research interests include satellite geodesy, GNSS, GNSS remote sensing.

Sandra Verhagen obtained her Ph.D. from and is now an assistant professor at the Delft University of Technology. Her research focuses on ambiguity resolution and integrity monitoring for real-time kinematic GNSS applications.